Green Chemistry

PAPER

View Article Online
View Journal

Cite this: DOI: 10.1039/d5gc04630k

Fallen-leaf-sensitized biosolar oxygenation of hydrocarbons

Minkyung Lee,†[a] Jinha Jang,†[a] Jeongeun Cha,[b] Sang Hyun Lee,[b] Frank Hollmann,[c] Keehoon Won *[d] and Chan Beum Park *[a]

Received 3rd September 2025,
Accepted 2nd January 2026

DOI: 10.1039/d5gc04630k

rsc.li/greenchem

Lignocellulosic wastes are naturally abundant carbon resources but have been underutilized due to their complex structure and recalcitrant nature. They require energy- and water-intensive processes, such as thermal, chemical, and/or mechanical pretreatments, for their valorization. Here, we report a new function of raw tree waste for driving the solar-powered oxygen reduction reaction (ORR) and biocatalytic oxyfunctionalization of hydrocarbons. We reveal that various lignocellulosic wastes, such as fallen leaves, waste wood, and wastepaper, can produce hydrogen peroxide (H_2O_2) using only O_2, water, and light without any pretreatment. In particular, fallen leaves from *Platanus* trees exhibit high rates of ORR, which is ascribed to their superior photophysical properties, such as higher light extinction, longer charge relaxation lifetime, and lower electron transfer resistance. We treated the fallen leaves of *Platanus* with H_2O_2-dependent unspecific peroxygenase to produce optically pure alcohols and epoxides through the stereoselective hydroxylation and epoxidation of hydrocarbons. The waste-enzyme hybrid catalyst achieved record-high turnover frequency and total turnover number. This study establishes raw biomass wastes as green photocatalysts for sustainable photobiosynthesis, presenting a successful example of waste-to-wealth conversion.

Green foundation

1. We show that untreated lignocellulosic wastes—especially fallen *Platanus* leaves—serve as biobased photocatalysts that reduce O_2 to H_2O_2 *via* a two-step $O_2^{\bullet-}$ pathway using only water and light; coupled with *Aae*UPO, these photocatalysts enable the biosolar oxyfunctionalization of hydrocarbons to achieve enantiopure alcohols/epoxides.
2. Fallen *Platanus* leaves photogenerated H_2O_2 at 360 ± 30 μM h^{-1} (≈2.6× kraft lignin), with EQEs of 74.4% (350 nm) and 49.8% (400 nm), sustaining ~1.2 mM over 48 h and retaining >210 μM h^{-1} upon reuse. Coupled *Aae*UPO under one-sun visible light, the system affords (*R*)-1-phenylethanol in >99% ee with TOF = 54 600 h^{-1} and TTN = 91 400 and epoxidation up to TTN = 133 500—without pretreatment or added sacrificial donors.
3. In our future studies, we plan (1) to move from the current pure O_2-purged, solar simulator-driven operations to air-fed, natural sunlight-driven ones and (2) to develop pilot-scale, higher-throughput flow processes for the greener production of high-value chiral chemicals.

Introduction

Approximately one billion tons of lignocellulosic wastes are produced annually as byproducts of agricultural practices.[1,2] These abundant natural carbon sources, which are primarily composed of lignin, cellulose, and hemicellulose, have attracted considerable interest as an alternative to dwindling fossil resources. Extensive research has been undertaken to separate their constituents from the robust composites of lignocellulosic biomass for utilization in chemicals and energy production.[3–6] However, the associated processes, including pretreatment, hydrolysis, and fermentation, are markedly energy-intensive and generate substantial wastewater.[7–9] Consequently, a growing body of research focuses on the direct utilization of this waste, circumventing the aforementioned complex procedures.[10,11]

Our group previously revealed that lignin separated from lignocellulosic biomass can function as a photocatalyst.[12] Lignin is a natural phenolic polymer composed of primary monomers, *p*-hydroxyphenyl (H), guaiacyl (G), and syringyl (S) units interconnected by C–C and/or C–O–C bonds. It shows exceptional light absorption and light-induced charge separ-

[a]*Department of Materials Science and Engineering, Korea Advanced Institute of Science and Technology (KAIST), 335 Science Road, Daejeon 34141, Republic of Korea. E-mail: parkcb@kaist.ac.kr*
[b]*Department of Biological Engineering, Konkuk University, 120 Neungdong-ro, Gwangjin-gu, Seoul 05029, Republic of Korea*
[c]*Department of Biotechnology, Delft University of Technology, Van der Maasweg 9, 2629 HZ Delft, Netherlands*
[d]*Department of Chemical and Biochemical Engineering, Dongguk University-Seoul, 30 Pildong-ro 1-gil, Jung-gu, Seoul 04620, Republic of Korea. E-mail: keehoon@dongguk.edu*
†These authors contributed equally to this work.

ation and transfer abilities and generates H_2O_2 *via* ORR using water as an eco-friendly electron donor. The fact that lignin is a major component (10%–50%) of lignocellulosic wastes[13,14] has motivated us to explore if lignocellulosic wastes can reduce O_2 to H_2O_2 using water as an electron donor under solar light. Remarkably, as presented in the current report, all tested lignocellulosic wastes, such as fallen leaves, waste wood, and wastepaper, generated H_2O_2, with the fallen leaves of *Platanus* trees displaying the highest rate—more than double that of lignin. To further understand the superior photocatalytic activity observed in the fallen leaves, comparative analyses involving Fourier transform infrared (FT-IR) spectroscopy, electrochemical impedance spectroscopy (EIS), cyclic voltammetry (CV), ultraviolet-visible (UV-vis) spectroscopy, chopped chronoamperometry (CA), and photoluminescence (PL) spectroscopy were conducted on isolated lignin. The photocatalytic mechanism of the fallen leaves for O_2 reduction to H_2O_2 was also thoroughly investigated.

Moreover, by combining the photocatalytic process for *in situ* H_2O_2 generation with unspecific peroxygenase from *Agrocybe aegerita* (*Aae*UPO),[15] a H_2O_2-dependent biocatalyst, bulk organic compounds were transformed into valuable building blocks (Fig. 1). The heme-thiolate enzyme catalyzes stereoselective hydroxylation and epoxidation reactions of hydrocarbons *via* the H_2O_2 shunt pathway,[16] producing pharmaceutical intermediates with high selectivity under mild conditions.[17] The remarkable photocatalytic performance of the fallen leaves was evidenced by significantly high turnover frequency (TOF) and total turnover number (TTN) metrics. This hybrid system achieves sustainable photobiosynthesis using only abundant, renewable, and cost-effective resources—waste, oxygen, water, and solar light—without necessitating energy-intensive pretreatments that produce pollutants. Our study shows that raw *Platanus* leaves act as efficient photocatalysts, as supported by photophysical and electrochemical analyses confirming effective photoexcitation, charge separation, and stepwise $O_2^{\bullet-}$-mediated ORR, enabling prolonged reactions and millimolar-level biocatalytic product formation. Unlike earlier biomass systems requiring sacrificial donors and producing additional chemical waste, our platform operates cleanly using only water with no pretreatment.[18,19]

Experimental section

Chemicals

H_2O_2 was purchased from Junsei Chemical Co., Ltd (Tokyo, Japan). Potassium phosphate monobasic, potassium phosphate dibasic, ethyl alcohol, D-(+)-xylose, calcium carbonate, sulfuric acid, and acetonitrile were purchased from Samchun Chemical Co., Ltd (Seoul, Korea). Kraft lignin, horseradish peroxidase (HRP), 2,2′-azino-bis(3-ethylbenzothiazoline-6-sulfonic acid) diammonium salt (ABTS), magnesium sulfate, dimethyl sulfoxide, ethyl acetate, 1-octanol, ethylbenzene,

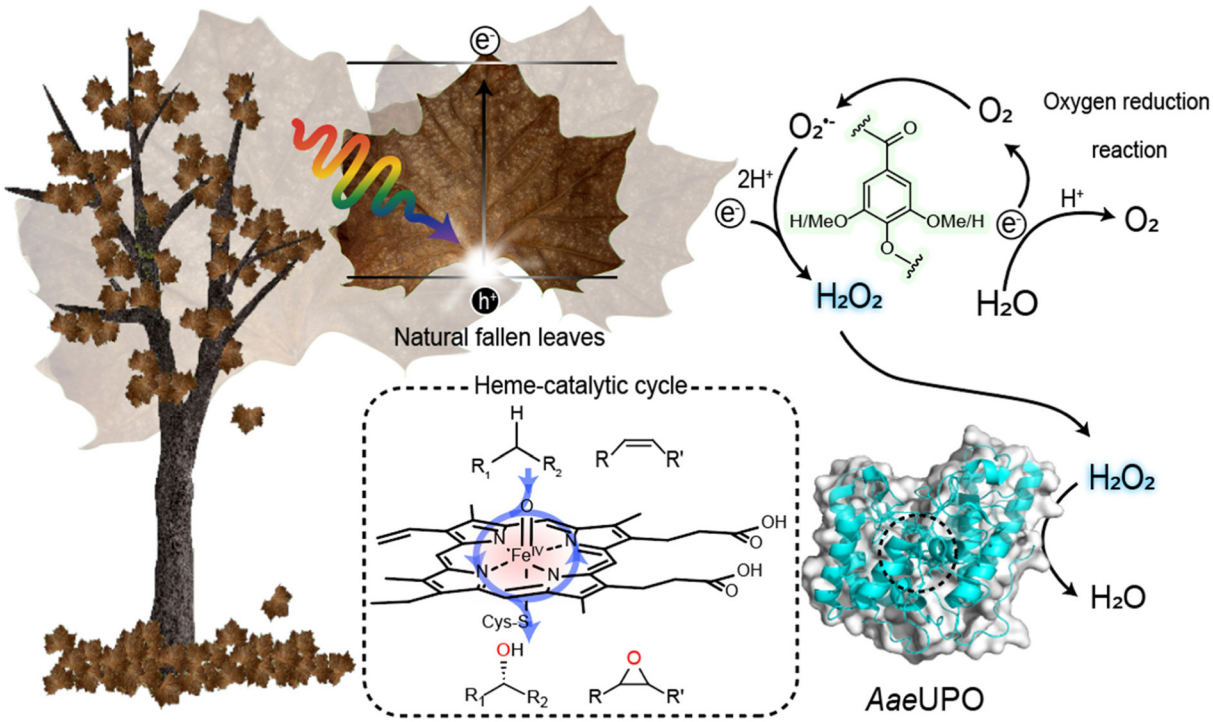

Fig. 1 Schematic of fallen leaf-driven sustainable photobiosynthesis. Biosolar oxyfunctionalization of C–H bonds using the composite of fallen leaves as photocatalyst and peroxygenase as biocatalyst. The photoexcited electrons and holes under a solar simulator participate in the reduction reaction of O_2 to H_2O. H_2O_2, generated through the photochemical reaction, reacts with substrates through peroxygenase, forming enantiopure products.

cis-β-methylstyrene, propylbenzene, cyclohexane, D-(+)-glucose, D-(+)-galactose, L-(+)-arabinose, D-(+)-mannose, ethylenediaminetetraacetic acid disodium salt dihydrate, silver nitrate, nitro blue tetrazolium, Nafion 117 solution, *p*-benzoquinone, 5,5-dimethyl-1-pyrroline *N*-oxide, citric acid, *tert*-butanol, and terephthalic acid were purchased from Sigma-Aldrich (St Louis, MO, USA). [Bmim][Ac] was purchased from BLD pharm (Shanghai, China). Waste wood from a wooden floor and softwood and hardwood powders were obtained from G-Biotech Co. (Sejong, Korea), and the wastepaper was a newspaper issued by Korea Advanced Institute of Science and Technology (KAIST, Daejeon, Korea). O_2 and N_2 gases (purity 99.999%) were bought from Special Gas Co. (Daejeon, Korea). A sieve (355 μm, *Φ*75 mm × 20 mm) was purchased from Chunggye Sieve Co. (Gunpo, Korea). Type 1 ultrapure water (18 MΩ cm) was used from a Direct-Q® 5 UV ultrapure water purification system (Millipore Corp., Burlington, MA, USA). *Aae*UPO was recombinantly expressed in *Komagataella phaffii* (also known as *Pichia pastoris*) on a pilot scale as described previously.[20,21]

Preparation of lignocellulosic powder samples

Fallen leaves of *Platanus*, pin oak, and red maple trees were collected at KAIST in December 2023. The leaves were gently washed with a deionized water-soaked sponge, dried in a vacuum desiccator at room temperature, and ground into fine powders. They were stored in a glass vial with a Teflon cap at room temperature.

Characterization of the fallen leaves

A V-750 UV-vis absorption spectrophotometer (JASCO, Tokyo, Japan) was utilized to estimate the energy band gap of the fallen *Platanus* leaves (0.1 mg mL^{-1} in KPi buffer (100 mM, pH = 7)). Tauc plots were acquired ($(\alpha h\nu)^2$ *versus* $h\nu$ where α, h, and ν represent the absorption coefficient, Planck's constant, and the photon frequency, respectively). A valence band X-ray photoelectron spectrometer (XPS) (AXIS Supra, Kratos Analytical, Manchester, UK; photon energy: 1486.6 eV (Al-Kα radiation)) was used to obtain the valence band maximum of the fallen *Platanus* leaves. Time-resolved fluorescence decay profiles were obtained to measure the charge carriers' lifetime in the powder samples using a Fluorolog®-3 spectrofluorometer (HORIBA, Kyoto, Japan) equipped with time-correlated single photon counting. An FT-IR spectrophotometer (Thermo Fisher Scientific, Waltham, MA, USA) was used to obtain FT-IR spectra and images. Sample morphologies were examined by scanning electron microscopy (SEM), and elemental composition/mapping was obtained by SEM-EDS (Hitachi, Japan). Surface chemical states were characterized by XPS (Al Kα, Thermo Fisher, USA), and specific surface area was determined from N_2 adsorption–desorption isotherms using the Brunauer–Emmett–Teller (BET) method.

NH_3- and CO_2-temperature-programmed desorption (TPD) analyses

TPD analyses were performed using a BEL/CAT2 instrument equipped with a TCD detector. For NH_3-TPD, ~60 mg of sample was pretreated in He (30 mL min^{-1}) at 120 °C for 80 min, cooled to 50 °C, and subsequently saturated with NH_3 (10% NH_3/He) for 1 h. The sample was then purged with He (30 mL min^{-1}) for 1 h to remove physisorbed NH_3, followed by desorption under a linear heating ramp from 50 to 300 °C at 10 °C min^{-1} while monitoring the signal using the TCD detector.

H_2O_2 quantification

Lignocellulosic powders and kraft lignin were dispersed by magnetic stirring in a KPi buffer (100 mM, pH = 7) with O_2 purging using a xenon arc lamp (260 nm < λ < 900 nm, I = 100 mW cm^{-2}) as the light source. The amount of H_2O_2 generated by the powder samples was determined using an ABTS assay. This colorimetric assay is based on the oxidation of ABTS catalyzed by HRP. A reaction sample (50 μL) was mixed with a colorimetric reagent solution (950 μl) containing 2 mM ABTS and 2.5 U HRP in a KPi buffer (100 mM, pH = 5). After shaking the resultant solution for 30 s, the absorbance at 420 nm was measured for H_2O_2 quantification using a V-750 spectrophotometer (JASCO, Tokyo, Japan).

Photoenzymatic reaction and analysis

A reaction mixture was prepared by dispersing the photocatalysts and substrates (ethylbenzene, *cis*-β-methylstyrene, propylbenzene, and cyclohexane) in a KPi solution (100 mM, pH = 7) and then adding *Aae*UPO with O_2 purging. The mixture was irradiated with a xenon arc lamp (I = 100 mW cm^{-2}) with a 400 nm cut-off filter (Newport) (400 nm < λ < 900 nm) to promote the visible light-driven UPO reaction. After the desired time, 50 μL of the reaction sample was withdrawn and mixed with 200 μL ethyl acetate (containing an internal standard of 5 mM 1-octanol) to extract the oxyfunctionalized products, and the residual water was then dried with $MgSO_4$. The concentrations of photoenzymatic reaction products were measured using a 7890A gas chromatograph equipped with a flame ionization detector (Agilent Technologies, Santa Clara, CA, USA) with a CP-Chirasil-Dex CB column (25 m × 3.2 cm × 0.25 μm). Detailed information about oven temperature programs is shown in Table S1. The ee, TOF, and TTN were calculated using eqn (1)–(3). TOF values were determined 30 min into the photoenzymatic reaction, while TTN and ee values were reported at the endpoint (48 h).

$$\text{ee} = (\text{moles of an enantiomer} - \text{moles of the other enantiomer}) / \text{total moles of product} \times 100 \quad (1)$$

$$\text{TOF}_{Aae\text{UPO}} = [\text{product}]/[Aae\text{UPO}] \times \text{time} \quad (2)$$

$$\text{TTN}_{Aae\text{UPO}} = \text{maximum [product] at a given time}/[Aae\text{UPO}] \quad (3)$$

Photoelectrochemical characterization

Photoelectrochemical analyses were conducted using a multichannel potentiostat (WMPG100, WonATech, Seoul, Korea)

and a xenon arc lamp (260 nm < λ < 900 nm, I = 100 mW cm^{-2}, AM 1.5G filter). The three-electrode system consisted of a glassy carbon electrode (GCE) as the working electrode, Ag/AgCl as the reference electrode, and platinum wire as the counter electrode. Powder samples were immobilized onto the GCE with Nafion 117. CV measurements were performed in a KPi electrolyte (100 mM, pH = 7, O_2 or N_2 saturated) for the fallen *Platanus* leaves and kraft lignin. CV curves were obtained in the region of −1.0 to 0.5 V (*vs.* Ag/AgCl) with a scan rate of 50 mV s^{-1}. EIS was performed in a KPi electrolyte (100 mM, pH = 7, O_2 saturated) using a ZIVE SP1 impedance analyzer (WonATech, Seoul, Korea) to examine the charge-transfer resistance of the fallen *Platanus* leaves and kraft lignin with an alternating current potential amplitude of 10 mV, frequency range from 100 kHz to 0.5 Hz, and applied bias of −0.6 V (*vs.* Ag/AgCl). Nyquist plots were made using the ZMAN software (WonATech, Seoul, Korea) and were fitted to a Randles circuit model, which consists of solution resistance (R_s), a constant phase element associated with the double layer capacitance (Q_{dl}), charge-transfer resistance (R_{ct}), and electrical components (Q_{ads} and R_{ads}) corresponding to the adsorption of reaction species.

In situ Raman spectroscopy

In situ Raman spectra were measured using a confocal Raman microscope (LabRAM HR Evolution, HORIBA, Kyoto, Japan) equipped with a 1064 nm laser. The fallen *Platanus* leaves (5 mg mL^{-1}) were dispersed in 30% (w/w) ACN/KPi (100 mM, pH = 7) with O_2 purging under a 395 nm light source (10 W). The spectra were obtained under blank, N_2/dark, N_2/light, O_2/dark, and O_2/light conditions.

Electron paramagnetic resonance (EPR) spectroscopy

To monitor the formation of superoxide radicals, we used a Bruker EMX plus 6/1 spectrometer with a frequency of 9.65 GHz. We prepared a reaction chamber with a KPi buffer (100 mM, pH = 7) containing 200 mM 5,5-dimethyl-1-pyrroline-*N*-oxide (DMPO) and the fallen *Platanus* leaves (5 mg mL^{-1}). EPR experiments were conducted by illuminating the reaction mixture with a visible-light flashlight under either O_2- or N_2-purged conditions using sealed gas bags. After 5 min of light exposure, the samples were immediately measured and put into an EPR cell. Measurement parameters were as follows: a microwave power of 3 mW, a modulation frequency of 100 kHz, and a modulation amplitude of 1.0 G at RT.

Dissolution of the fallen *Platanus* leaves followed by reassembly

After grinding and ultrasonicating the fallen *Platanus* leaves in 70% (v/v) ethanol/deionized water for 1 h, the resultant powders (5 mg) were added to 10 mL of [Bmim][Ac] and stirred at 700 rpm and 90 °C. After complete dissolution, deionized water was poured as an anti-solvent into the homogeneous ionic liquid solution. As a result, the water-insoluble components of the fallen *Platanus* leaves were precipitated and separated by centrifugation (13 000 rpm, 10 min), followed by drying in a vacuum oven.

Compositional analysis

Each lignocellulosic waste (0.5 g) was washed with ethanol (100 mL) three times, followed by another three washes with deionized water (100 mL) to eliminate extractives using vacuum filtration. Then, the washed powders were dried at 60 °C and allowed to cool in a desiccator to room temperature, and the extractive content was quantified. The washed powders were ground with a pestle and ceramic mortar and passed through a 42-mesh sieve, and only particles finer than 42 mesh were retained for subsequent analysis.

The chemical composition of the pretreated biomass was determined according to the NREL method,[22] with slight modifications based on Toda *et al.*'s findings.[23] For analysis, 75 mg of the sample (10% w/v) was hydrolyzed with 72% (w/w) sulfuric acid at 30 °C for 3 h with shaking at 120 rpm. The acid concentration was then reduced to 4% by adding deionized water, and the mixture was autoclaved at 121 °C for 30 min. After cooling, the samples were filtered under vacuum using a 25 mL porcelain porous filter crucible.

The acid-soluble lignin content in the filtrate was measured at 240 nm using a UV-vis spectrophotometer with an absorptivity coefficient of 110 l g^{-1} cm^{-1} eqn (4). The filtrate was neutralized to a pH of 7 by adding calcium carbonate, then stored overnight at 4 °C to precipitate the insoluble fraction. The clear supernatant was separated by centrifugation for subsequent analysis. Hydrolyzed sugar monomers were quantified using an HPLC equipped with a refractive index detector (Shimadzu, Kyoto, Japan) and a Shodex SUGAR SP0810 column. The mobile phase was water at a flow rate of 0.6 mL min^{-1} with an injection volume of 10 μL. The column was maintained at 80 °C, and the detector was set at 35 °C. Standards included glucose, xylose, galactose, arabinose, and mannose. The glucan content was calculated by multiplying the total glucose content by a conversion factor of 0.9 to account for water release during polymerization. The hemicellulose content was determined by summing the amounts of xylose, galactose, arabinose, and mannose and applying conversion factors of 0.88 for C-5 sugars and 0.9 for C-6 sugars.

Filters containing acid-insoluble lignin and ash were washed with 60 °C distilled water, dried overnight at 60 °C, weighed, and then ignited in a muffle furnace at 525 °C for 18 h. The cooled filters were then weighed to determine the ash content eqn (5). All analyses were performed in triplicate to obtain the results.

$$\text{Acid soluble lignin}\,(\%) = \frac{\frac{\text{OD}_{240\,\text{nm}}}{c \times \text{absorptivity}} \times \text{df} \times V}{\text{total weight}} \times 100 \quad (4)$$

c = cell length, df = dilution factor, V = volume.

$$\text{Acid insoluble lignin}\,(\%) = \frac{w_1 - w_2}{\text{total weight}} \times 100 \quad (5)$$

w_1 = acid insoluble lignin + acid insoluble ash; w_2 = acid insoluble ash.

Hydrochar preparation of *Platanus* leaves

Hydrochar was prepared from the dried *Platanus* leaf powder following a modified hydrothermal carbonization procedure.[24,25] Briefly, 1 g of leaf powder was suspended in 40 mL of deionized water and mixed for 30 min. Citric acid (25 mg) was then added and allowed to dissolve under continuous stirring. The resulting mixture was transferred into a 50 mL Teflon-lined stainless-steel autoclave and heated at 200 °C for 24 h. After naturally cooling to room temperature, the solid product was collected, thoroughly washed several times with deionized water and ethanol, and dried at 70 °C for 12 h to yield the hydrochar.

Results and discussion

Characterization and screening of lignocellulosic waste

We investigated various fallen leaves from trees (*e.g.*, *Platanus*, pin oak, and red maple), waste wood, wastepaper, and wood powders (*e.g.*, hardwood and softwood) as lignocellulosic wastes, alongside kraft lignin as a positive control. The powder images of the lignocellulosic materials and kraft lignin are shown in Fig. S1. According to our analysis using FT-IR spectroscopy (Fig. 2a and Fig. S2), a strong peak associated with the C=O group[26] was distinctly observed in the range of 1600–1700 cm^{-1}, and the peak of the G unit characteristic of lignin[27] appeared at around 1150–1250 cm^{-1}. In addition, we performed compositional analyses of the lignocellulosic wastes according to the US National Renewable Energy Laboratory (NREL)[28–30] protocol. Our compositional analysis revealed that fallen *Platanus* leaves and wastepaper contain the highest (46.6% $w/w_{dry\ weight}$) and the lowest (8.8% $w/w_{dry\ weight}$) lignin contents, respectively (Table S2). We conducted characterization of the fallen *Platanus* leaves. The SEM image showed a length-based particle-size distribution for the ground photocatalyst with typical lengths of 10–20 μm (Fig. 2b); SEM-EDS quantified the elemental composition and relative ratios (Fig. S3a), XPS spectra were dominated by C 1s and O 1s features (Fig. S3b), and BET analysis gave a specific surface area of 0.284 $m^2\ g^{-1}$.

We assessed the potential of various lignocellulosic wastes for photocatalytic O_2 reduction to H_2O_2 under O_2 purging and illumination. As shown in Fig. 2c, remarkably, all the tested lignocellulosic wastes generated H_2O_2, with fallen *Platanus* leaves exhibiting the highest H_2O_2 production rate (360 ± 30 μM h^{-1}) which was more than twice that of kraft lignin (140 ± 10 μM h^{-1}). We found positive correlations of the H_2O_2 generation rate with the concentration (1, 3, and 5 mg mL^{-1}) and light intensity (100 and 200 mW cm^{-2}), which indicate a light-dependent catalytic function of the leaves for H_2O_2 formation (Fig. 2d). The decreased H_2O_2 generation beyond the concentration of 5 mg mL^{-1} is ascribed to a self-shading effect, reducing the catalytic active sites available for oxygen reduction.[31,32] Under monochromator-selected illumination at 350 and 400 nm (10 mW cm^{-2}, illuminated area 4.24 cm^2, 30 min), the fallen *Platanus* leaves (1 mg mL^{-1}) showed EQEs of 74.4% and 49.8%—approximately4.0× and ~4.7× higher than those of kraft lignin (18.4% and 10.6%)—demonstrating superior photon utilization (eqn (6) in the SI and Fig. S4). As shown in Fig. S5a, the *Platanus* leaves (1 mg mL^{-1}) exhibited a continuous increase in H_2O_2 production over 48 h, ultimately generating approximately 1.2 mM of H_2O_2. The fallen *Platanus* leaves consistently exhibited higher photocatalytic activity (>210 μM h^{-1}) during repeated use, underscoring their excellent durability and reusability as a biobased photocatalyst (Fig. S5b). Control experiments under dark or N_2 conditions showed negligible H_2O_2 formation, suggesting both light and O_2 are key for the redox reaction (Fig. 2e). The C 1s and O 1s XPS spectra of the *Platanus* leaves remained essentially unchanged before and after photocatalysis (Fig. S6), indicating no detectable alteration of the leaf surface composition under the reaction conditions.

Photocatalytic properties of fallen *Platanus* leaves

To elucidate the underlying mechanism for the enhanced photocatalytic H_2O_2 production by the fallen *Platanus* leaves, we investigated their photophysical and photoelectric properties. Comparison of the UV-vis spectrum of the fallen *Platanus* leaves with that of kraft lignin (Fig. 3a) revealed a higher light extinction of the fallen *Platanus* leaves in the 250–700 nm range. To investigate the separation lifetime of photoexcited electron–hole pairs, we conducted time-resolved photoluminescence (TRPL) spectroscopic analysis. The TRPL decay profiles showed that the average fluorescence lifetimes of the fallen *Platanus* leaves (1.9 ns and 1.5 ns) were significantly longer than those of kraft lignin (1.0 ns and 0.48 ns) at photoexcitation wavelengths of 264 nm and 316 nm, respectively (Fig. 3b and Fig. S7), indicating that the fallen *Platanus* leaves undergo slower charge recombination. To examine the charge-transfer resistance (R_{ct}) of the photoexcited electrons, we used EIS analysis of the powder samples dispersed in O_2-saturated KPi (100 mM, pH = 7) under light. The R_{ct} value of the fallen *Platanus* leaves (41.5 kΩ) was much lower than that of lignin (103 kΩ) according to the Nyquist plots, which were fitted to a Randles circuit model (Fig. 3c). Furthermore, CV comparison revealed a more cathodic ORR peak[33] and lower current values for kraft lignin than the fallen *Platanus* leaves (Fig. S8). Among the defoliated leaf samples, *Platanus* leaves exhibited the highest photocurrent in chopped CA measurements, indicating their superior photoresponse under illumination (Fig. S9). These results support that (1) higher light absorption, (2) a longer charge relaxation lifetime, and (3) a lower electron transfer resistance enable a higher photocatalytic production rate of H_2O_2 for the fallen *Platanus* leaves.

We hypothesized that the elaborate heterostructure formed by lignin and other constituents within the fallen *Platanus* leaves facilitates effective separation of photogenerated electrons and holes, leading to their superior photocatalytic properties. To verify this hypothesis, TPD analysis was conducted (Fig. S10). The results showed that the acidic and basic site densities of kraft lignin, *Platanus* leaves, and softwood did not correlate with their H_2O_2 production, indicating that the superior $2e^-$ ORR activity of *Platanus* leaves is governed by photophysical

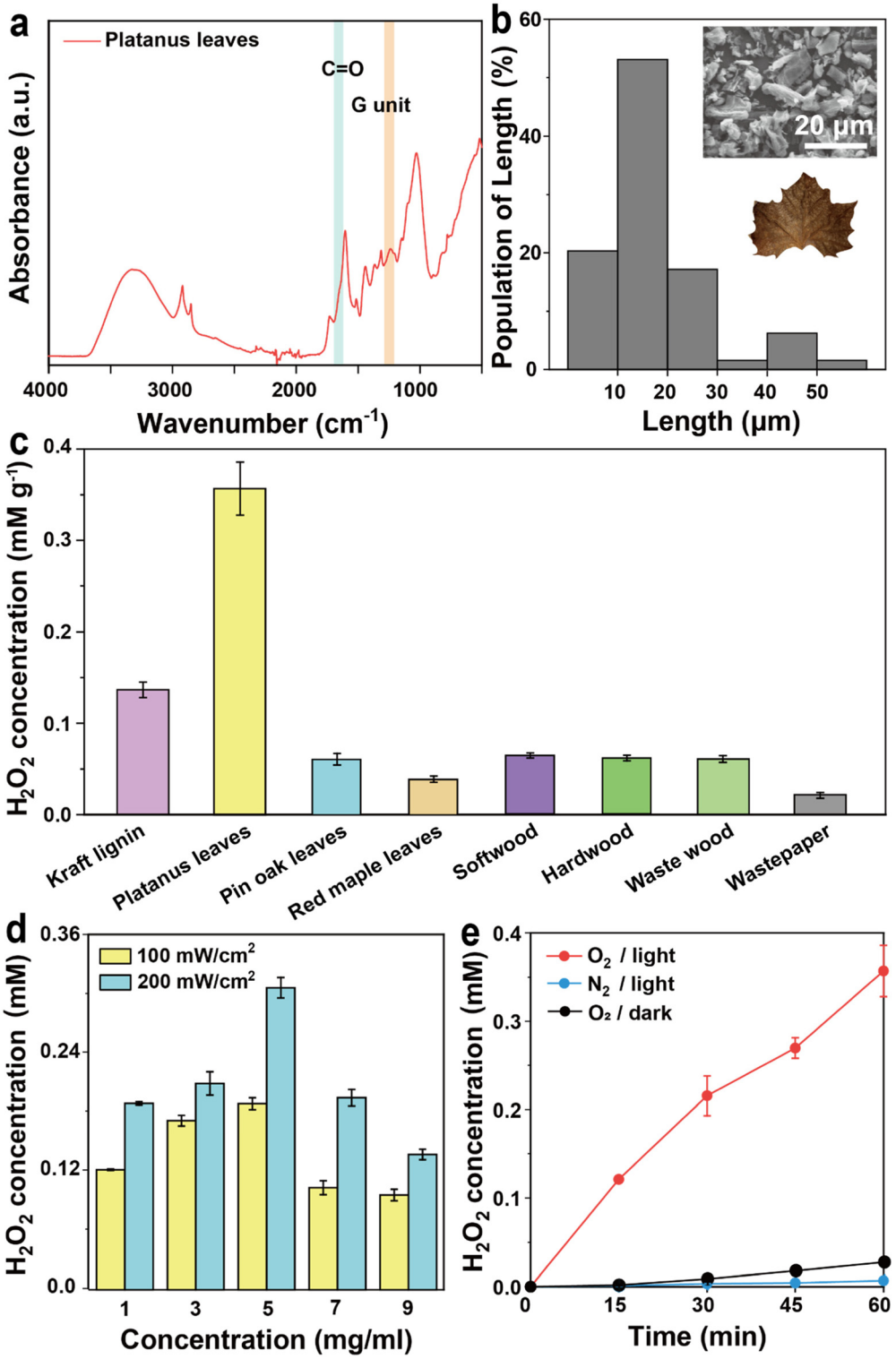

Fig. 2 Lignocellulosic waste-induced H_2O_2 production under light. (a) FT-IR spectrum of the fallen *Platanus* leaves. (b) SEM image and size distribution of the ground fallen *Platanus* leaves. (c) H_2O_2 production by kraft lignin and various lignocellulosic wastes as photocatalysts (1 mg mL^{-1}) under light (260 nm < λ < 900 nm, I = 100 mW cm^{-2}) in a KPi buffer (100 mM, pH = 7) with O_2 purging at room temperature for 1 h. (d) H_2O_2 production at different concentrations of the fallen *Platanus* leaves and light intensities (260 nm < λ < 900 nm) in a KPi buffer (100 mM, pH = 7) with O_2 purging at room temperature for 15 min. (e) Time profiles of H_2O_2 production by the fallen *Platanus* leaves (1 mg mL^{-1}) in a KPi buffer (100 mM, pH = 7) under O_2/light, N_2/light, or O_2/dark conditions (260 nm < λ < 900 nm, I = 100 mW cm^{-2}) at room temperature.

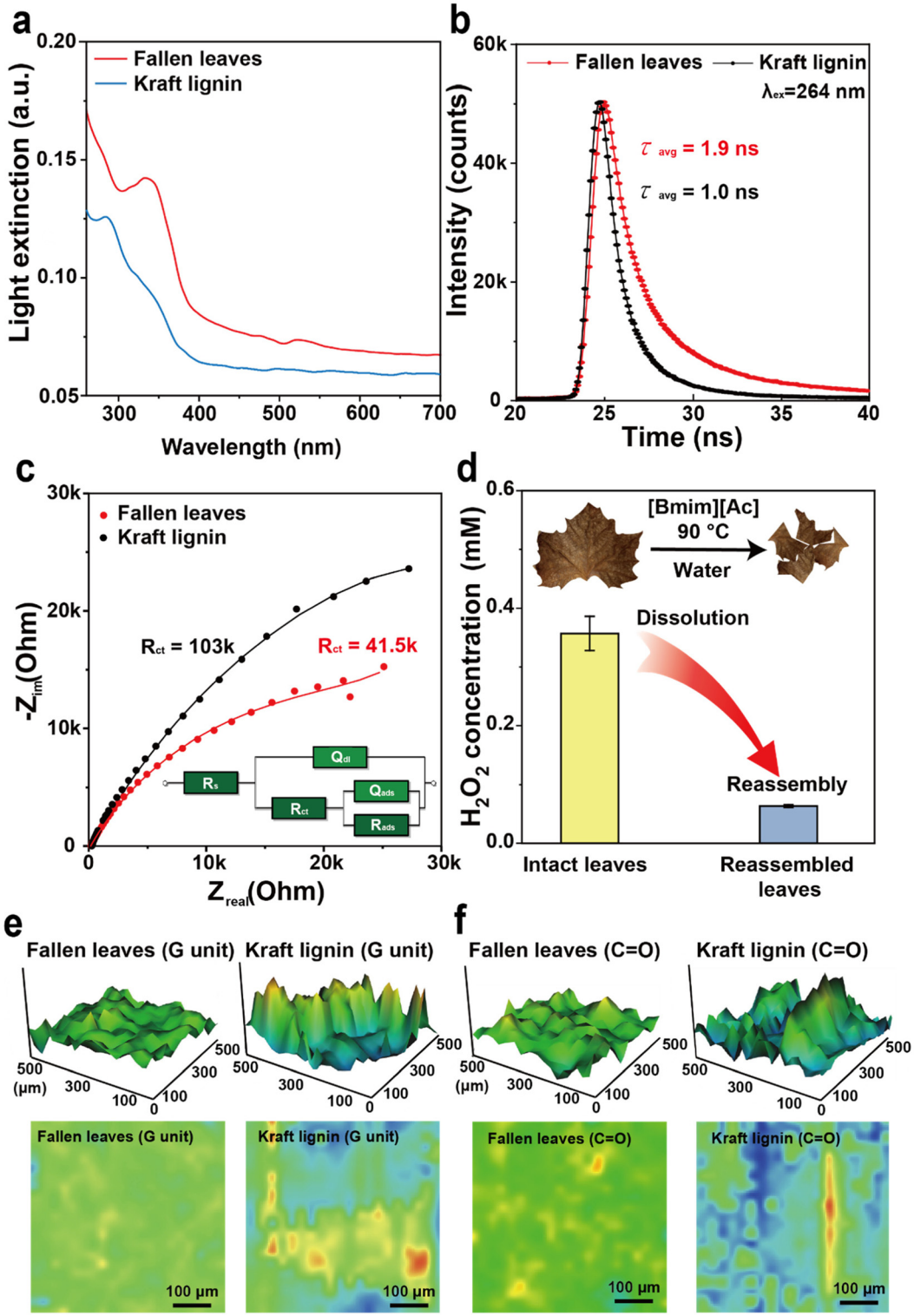

Fig. 3 Photocatalytic properties of the fallen *Platanus* leaves and kraft lignin. (a) UV-vis spectra of the fallen *Platanus* leaves and kraft lignin (0.01 mg mL^{-1}). (b) Time-resolved fluorescence decay profiles of the fallen *Platanus* leaves (red) and kraft lignin (black) at excitation wavelength = 264 nm in KPi (100 mM, pH = 7). Powder concentration: 0.1 mg mL^{-1}. These decay profiles were fitted to a quadruple-exponential function; the fallen *Platanus* leaves: τ_1 = 1.9 ns, τ_2 = 3.4 ns, and τ_3 = 12.1 ns, τ_4 = 1.9 ns with average fluorescence lifetime = 1.9 ns; kraft lignin: τ_1 = 0.7 ns, τ_2 = 0.2 ns, and τ_3 = 2.0 ns, τ_4 = 6.3 ns with average fluorescence lifetime = 1.0 ns. (c) Nyquist plots of the fallen *Platanus* leaves and kraft lignin under light (260 nm < λ < 900 nm, I = 100 mW cm^{-2}) in an O_2-saturated Kpi buffer (100 mM, pH = 7) at −0.6 V (*vs.* Ag/AgCl). Z_{real} and Z_{im} represent real and imaginary impedances, respectively. (d) H_2O_2 production by the intact and reassembled leaves in a Kpi buffer (100 mM, pH = 7) under light with O_2 purging. (e) FT-IR 3D and 2D images for the G unit of the fallen *Platanus* leaves and kraft lignin (1150–1250 cm^{-1}). (f) FT-IR 3D and 2D images for conjugated C═O group of the fallen *Platanus* leaves and kraft lignin (1600–1700 cm^{-1}).

and structural factors rather than acid–base site abundance. Next, we dissolved the fallen *Platanus* leaves using an ionic liquid to disrupt their heterostructure. After physical pretreatments of grinding and ultrasonication, they were dissolved in 1-butyl-3-methylimidazolium acetate ([Bmim][Ac]) with stirring at 90 °C.[34] Then, we added deionized water as an anti-solvent[35] to the ionic liquid solution to recover their components (Fig. S11). These reassembled fallen *Platanus* leaves exhibited a drastically lower photocatalytic H_2O_2 generation activity (63 ± 3 μM h^{-1}) than the intact ones (Fig. 3d), which implies that the specific heterogeneous architecture within the fallen *Platanus* leaves is crucial for their superior photocatalytic activity.

Molecular catalysts can form self-aggregates through various molecular interactions (*i.e.*, π–π stacking interaction, hydrogen bonding, and van der Waals interactions).[36,37] The self-aggregation considerably reduces their catalytic activity by quenching excited states, altering their redox properties, and/or lowering the fraction of active molecules for catalysis. Lignin molecules also aggregate *via* π–π interactions and hydrogen bonding. Our group recently found that suppressing the self-aggregation of lignin is an efficient means of enhancing its photocatalytic activity for H_2O_2 generation.[38] In the present study, we examined the degree of self-aggregation of lignin within the fallen *Platanus* leaves by measuring the distribution of its specific functional groups, such as the G unit, through FT-IR imaging. As shown in Fig. 3e, the G unit (1150–1250 cm^{-1}) is more uniformly present in the fallen *Platanus* leaves than in kraft lignin, indicating a lower degree of self-aggregation of lignin within the fallen *Platanus* leaves. We further investigated the spatial distribution of conjugated carbonyl groups (1600–1700 cm^{-1}), which are active sites of metal-free organic photocatalysts for ORR.[26,39,40] The FT-IR images revealed that the carbonyl group was uniformly distributed in the fallen *Platanus* leaves, unlike lignin (Fig. 3f). The other lignocellulosic wastes, which showed low ORR rates, exhibited significant spatial variations of the G unit and C=O group like kraft lignin (Fig. S12). These results show that the lower self-aggregation of lignin and carbonyl groups within the fallen *Platanus* leaves induces higher photocatalytic activity. Additionally, confocal microscopy showed that ionic-liquid dissolution and regeneration collapsed the native cell-wall architecture (bright lines) of fallen *Platanus* leaves (Fig. S13a and b). FT-IR imaging revealed that guaiacyl (G) units and conjugated C=O groups, uniform before processing, became aggregates after reassembly, resembling other lignocellulosic wastes (Fig. S13c and d). Hydrothermal conversion of *Platanus* leaves into hydrochar increased both H_2O_2 production and the O 1s XPS signal (Fig. S14a–e), indicating that the introduction of additional oxygenated functional groups can further enhance performance, serving as a potential complementary strategy beyond the intrinsic photocatalytic activity of the native leaves.

Photoelectron transfer from fallen *Platanus* leaves to O_2 into H_2O_2

We investigated the photocatalytic electron transfer mechanism of the fallen *Platanus* leaves for ORR. First, we analyzed their conduction band minimum (CBM) energy potential to ensure that the fallen *Platanus* leaf-driven O_2 reduction to H_2O_2 is thermodynamically feasible. The CBM was calculated from the valence band maximum (VBM) and the energy gap between VBM and CBM. The band gap of the fallen *Platanus* leaves was estimated to be 3.1 eV according to the Tauc plots [$(\alpha h\nu)^2$ *vs.* $h\nu$] from light extinction using UV-vis spectroscopy (Fig. S15a). We used valence-band X-ray photoelectron spectroscopy (Fig. S15b) to estimate their VBM energy potential, finding it to be 2.918 V (*vs.* reversible hydrogen electrode, RHE). Based on their energy bandgap and VBM, we calculated their CBM to be −0.182 V (*vs.* RHE). Because the leaves' CBM is more negative than the reduction potential (E_{red}) of O_2 to H_2O_2 (0.68 V *vs.* RHE), the transfer of electrons photoexcited from the fallen *Platanus* leaves to O_2 into H_2O_2 [$O_2 + 2(H^+ + e^-) \rightarrow H_2O_2$] is thermodynamically favorable (Fig. S15c). In addition, we examined the other half-reaction to sustain the whole redox reaction. The VBM of the fallen Platanus leaves (2.918 V *vs.* RHE) is positive enough for the favorable oxidation of H_2O to O_2 (1.23 V *vs.* RHE) [$2H_2O \rightarrow O_2 + 4(H^+ + e^-)$].

The O_2 reduction to H_2O_2 can occur *via* (i) a two-step ($O_2 \rightarrow O_2^{\bullet-} \rightarrow H_2O_2$) single-electron transfer and/or (ii) a one-step ($O_2 \rightarrow H_2O_2$) two-electron transfer reaction[12,41] (Fig. 4a). To verify the electron transfer pathway of the fallen *Platanus* leaf-driven O_2 reduction, we analyzed the formation of $O_2^{\bullet-}$, an intermediate of the two-step ORR pathway. Addition of *p*-BQ as an $O_2^{\bullet-}$ scavenger to the reaction medium significantly decreased the H_2O_2 generation rate (Fig. 4b), which indicates $O_2^{\bullet-}$ is produced during the reaction. To examine the possible involvement of hydroxyl radicals,[42] we performed *tert*-butanol scavenger tests (0%, 5%, 50% v/v), which showed no change in H_2O_2 production, indicating that $^{\bullet}OH$ does not participate in the two-electron ORR (Fig. S16). However, terephthalic acid (TA) fluorescence assays revealed that $^{\bullet}OH$ is generated during illumination: 2-hydroxyterephthalic acid (HTA) fluorescence increased under O_2/light conditions and under N_2/light conditions with 100 μM of additional H_2O_2, confirming formation through water oxidation and H_2O_2 decomposition (Fig. S17a and b). These parallel $^{\bullet}OH$ formation pathways are summarized in Fig. S17c.

In addition, we employed vibrational spectroscopic techniques, such as EPR and *in situ* Raman spectroscopy, to detect $O_2^{\bullet-}$. For EPR spectroscopy, we dispersed the fallen *Platanus* leaves (5 mg mL^{-1}) in a KPi buffer (100 mM, pH = 7) and added 200 mM DMPO as a spin trap.[43,44] After the photochemical reaction under O_2 conditions, the characteristic peaks of DMPO-OH (*) and DMPO-OOH were simultaneously detected, whereas no significant peaks were observed before the reaction and under N_2 conditions (Fig. 4c). For *in situ* Raman spectroscopy, we used a 1064 nm laser despite its low sensitivity because of the inherent fluorescence properties of the fallen *Platanus* leaves. To compensate for the low sensitivity of the laser, acetonitrile (ACN) was added as a cosolvent[45] to a KPi buffer (100 mM, pH = 7), extending the lifetime of $O_2^{\bullet-}$ (Fig. S18). We confirmed the presence of $O_2^{\bullet-}$ only under positive conditions, as evidenced by its characteristic peak[46] at

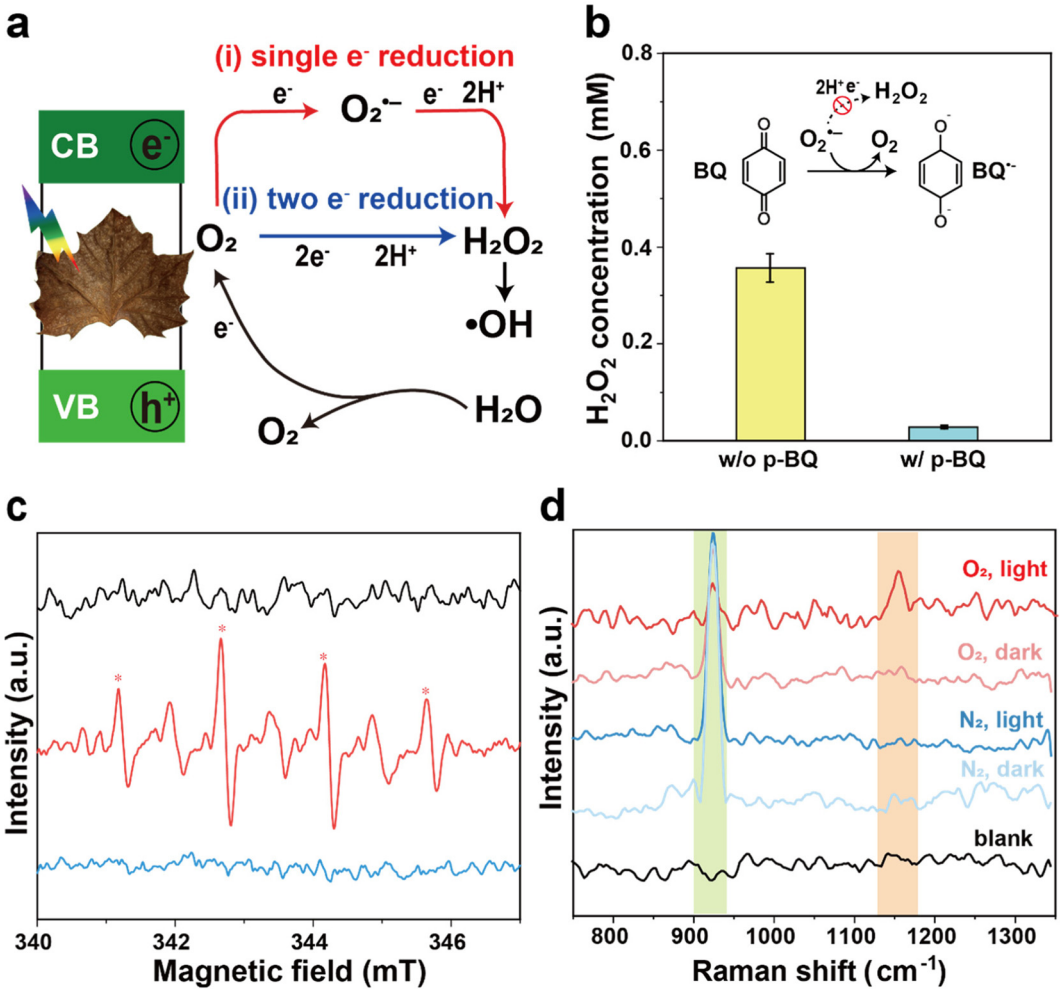

Fig. 4 Mechanism of the fallen *Platanus* leaf-driven H_2O_2 generation under light. (a) Illustration of O_2 reduction reaction to H_2O_2 by two possible pathways. (b) Effect of *p*-BQ on the rate of photocatalytic H_2O_2 production. Reaction conditions: fallen *Platanus* leaves (1 mg mL^{-1}) with or without *p*-BQ (100 mM) in a KPi buffer (100 mM, pH = 7) upon O_2 purging at room temperature. (c) EPR before (black) and after the photocatalytic reaction under O_2/light (red) or N_2/light (blue). Reaction time: 10 min. Spin trapping agent: 5,5-dimethyl-1-pyrroline-N-oxide. (d) *In situ* Raman spectra with or without O_2, light, and photocatalyst (5 mg mL^{-1}) using a 1064 nm laser. Green region: aromatic rings, red region: $O_2^{\bullet-}$.

1130 cm^{-1} in Fig. 4d. Taken together, we concluded that the photocatalytic O_2 reduction by the fallen *Platanus* leaves occurs dominantly through the two-step single-electron transfer pathway involving an $O_2^{\bullet-}$ intermediate.

Enantioselective photobiocatalytic oxyfunctionalization by leaves and peroxygenase

UPOs catalyze stereoselective hydroxylation and epoxidation of inert C–H bonds using H_2O_2 as an oxidant under mild conditions, which makes them a promising alternative to cytochrome P450 monooxygenases and their chemical counterparts.[12] However, they suffer from the oxidative degradation and irreversible inactivation of their heme active sites at elevated concentrations of H_2O_2, which necessitates an *in situ* H_2O_2 supply.[47] For this purpose, we combined *in situ* H_2O_2 generation by the fallen leaf photocatalyst with oxyfunctionalization by *Aae*UPO biocatalyst to transform organic compounds into value-added chemicals. The leaf/*Aae*UPO-driven oxyfunctionalization in a one-pot process was performed using a 400 nm filter to harness visible light, which constitutes almost half of the sunlight spectrum,[48] under one sun illumination (I = 100 mW cm^{-2}) to demonstrate actual artificial photobiosynthesis. Lignin, owing to its assembly of conjugated quinone- and carbonyl-type chromophores, can absorb photons in the visible region[49,50] and thus be directly photoexcited under our reaction conditions.

For the photoenzymatic oxygenation of ethylbenzene to (*R*)-1-phenylethanol, the amount of H_2O_2 generated at an optimal concentration of 5 mg mL^{-1} is presented in Fig. S19. The fallen *Platanus* leaves achieved the highest TOF of 54 600 h^{-1} for *Aae*UPO at an optimal concentration of 5 mg mL^{-1}, outperforming their counterpart, kraft lignin (Fig. 2c and Fig. S20). The fallen *Platanus* leaves supplied H_2O_2 to *Aae*UPO, leading to the continuous production of (*R*)-1-phenylethanol for 48 h under optimal conditions with a high enantiomeric excess (ee) of >99% and a TTN of 91 400 (Fig. S21a). Neither over-oxi-

dation of (*R*)-1-phenylethanol to acetophenone nor racemic reaction was observed, unlike in other studies[51–53] (Fig. S21b). Control experiments without O_2, leaves, *Aae*UPO, or substrate resulted in negligible formation of products (Fig. 5b). Furthermore, to examine the effect of enzyme concentration on the production of hydroxylated products, we compared the concentration of (*R*)-1-phenylethanol over 48 h at enzyme loadings of 10, 50, and 100 nM. The final concentrations of (*R*)-1-phenylethanol reached 0.91, 1.61, and 2.90 mM, respectively, clearly demonstrating that product formation increased with higher enzyme concentrations (Fig. S22). In the photoenzymatic reaction, both the TTN and TOF values of the fallen *Platanus* leaves surpassed those obtained with kraft lignin as well as with the representative photocatalysts g-C_3N_4 and TiO_2 (Fig. S23). In particular, the TOF value was approximately 3-, 12-, and 52-fold higher than those of kraft lignin, g-C_3N_4, and TiO_2, respectively.

Finally, we successfully tested the general applicability of the leaf-*Aae*UPO hybrid catalysts to other oxyfunctionalization reactions such as enantioselective epoxidation of *cis*-β-methylstyrene (TOF = 51 900 h^{-1}, TTN = 133 500, and ee > 99%) and hydroxylation of propylbenzene (TOF = 12 000 h^{-1}, TTN = 10 000, and ee > 99%) and cyclohexane (TOF = 6200 h^{-1} and TTN = 12 900). Fig. 5c shows that the leaf photocatalyst is compatible with a broad range of oxyfunctionalization substrates with TTNs (>10 000). Overall, we demonstrated that waste-based photoenzymatic reactions achieve record-high TOF and TTN values.

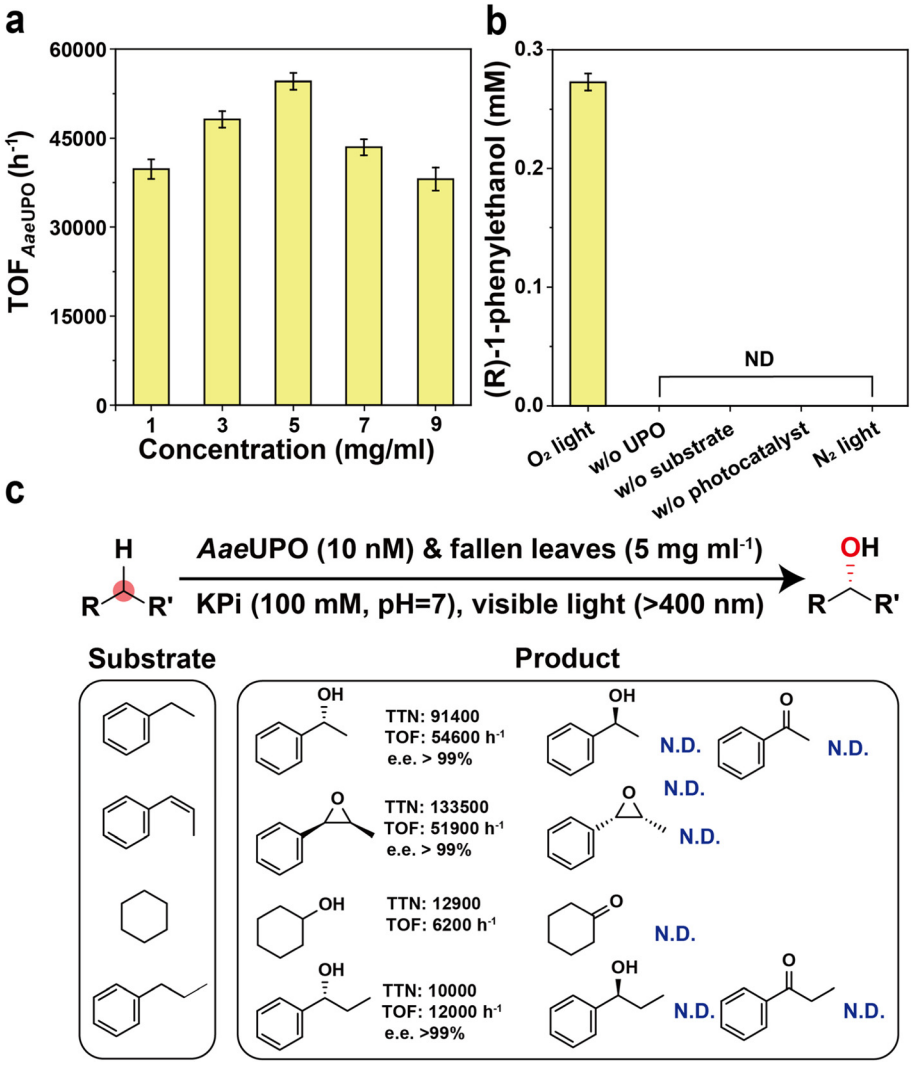

Fig. 5 Photobiocatalytic oxyfunctionalization reaction using the fallen *Platanus* leaf photocatalyst and *Aae*UPO biocatalyst. (a) Production rate of (*R*)-1-phenylethanol with different concentrations of the fallen *Platanus* leaves under visible light (400 nm < λ < 900 nm, I = 100 mW cm^{-2}) in a KPi buffer (100 mM, pH = 7) upon O_2 purging with 10 nM *Aae*UPO and 10 mM ethylbenzene after 30 min. (b) Control experiments of (*R*)-1-phenylethanol production by the fallen *Platanus* leaves (5 mg mL^{-1}) after 30 min. (c) Reaction equation of the biosolar oxyfunctionalization by the fallen *Platanus* leaf/*Aae*UPO. Reaction substrates (ethylbenzene, *cis*-β-methylstyrene, cyclohexane, and propylbenzene) and their products with TTN, TOF, and ee.

Conclusions

We have substantiated creative upcycling of raw lignocellulosic wastes into valuable photocatalysts for O_2 reduction to H_2O_2 without conventional pretreatments. In addition, we have integrated the waste-driven photocatalysis with H_2O_2-dependent biocatalysis to produce value-added enantiopure alcohols and epoxides. The lignin-containing wastes, such as fallen leaves, waste wood, and waste paper, reduced O_2 to H_2O_2 under illumination without any additional electron donor (*e.g.*, methanol, formic acid, TEOA) *via* a two-step single-electron transfer pathway ($O_2 \rightarrow O_2^{\bullet-} \rightarrow H_2O_2$). The fallen leaves of *Platanus* trees were notable for their superior photoreduction ability, outperforming lignin isolated through energy-intensive pretreatments. They exhibit higher light extinction, longer charge relaxation lifetime, and lower electron transfer resistance with uniform distribution of functional groups (*i.e.*, G unit and conjugated C=O group) than other lignocellulosic wastes. Furthermore, the combination of the leaves and *Aae*UPO catalyzed enantio- and chemo-selective oxygenation reactions of various hydrocarbons under solar light with record-high catalytic metrics. This work shows successful waste-to-wealth conversion using untreated wastes as green photocatalysts for light-driven oxygenation of hydrocarbons, realizing sustainable photobiosynthesis.

Conflicts of interest

There are no conflicts to declare.

Data availability

The data supporting this article have been included as part of the supplementary information (SI). Supplementary information is available. See DOI: https://doi.org/10.1039/d5gc04630k.

Acknowledgements

This work was supported by the National Research Foundation of Korea (NRF) grants funded by the Ministry of Science and ICT (Grant No. RS-2023-00222078, RS-2024-00440681, RS-2024-00460425). F. H. acknowledges funding from the European Union (ERC, PeroxyZyme, No. 101054658).

References

1 S. Periyasamy, V. Karthik, P. Senthil Kumar, J. B. Isabel, T. Temesgen, B. M. Hunegnaw, B. B. Melese, B. A. Mohamed and D.-V. N. Vo, *Environ. Chem. Lett.*, 2022, **20**, 1129–1152.
2 C. Tian, R. Dorakhan, J. Wicks, Z. Chen, K.-S. Choi, N. Singh, J. A. Schaidle, A. Holewinski, A. Vojvodic, D. G. Vlachos, L. J. Broadbelt and E. H. Sargent, *Nat. Catal.*, 2024, **7**, 350–360.
3 F. Xu, J. Sun, N. V. S. N. M. Konda, J. Shi, T. Dutta, C. D. Scown, B. A. Simmons and S. Singh, *Energy Environ. Sci.*, 2016, **9**, 1042–1049.
4 E. Feghali, G. Carrot, P. Thuéry, C. Genre and T. Cantat, *Energy Environ. Sci.*, 2015, **8**, 2734–2743.
5 B. Liang, J. Yang, C. F. Meng, Y. R. Zhang, L. Wang, L. Zhang, J. Liu, Z. C. Li, S. Cosnier, A. H. Liu and J. M. Yang, *Nat. Commun.*, 2024, **15**, 8764.
6 X. Wu, X. Fan, S. Xie, J. Lin, J. Cheng, Q. Zhang, L. Chen and Y. Wang, *Nat. Catal.*, 2018, **1**, 772–780.
7 L. Xu, M. Cao, J. Zhou, Y. Pang, Z. Li, D. Yang, S. Y. Leu, H. Lou, X. Pan and X. Qiu, *Nat. Commun.*, 2024, **15**, 734.
8 R. J. Patinvoh, O. A. Osadolor, K. Chandolias, I. Sarvari Horvath and M. J. Taherzadeh, *Bioresour. Technol.*, 2017, **224**, 13–24.
9 Z. H. Liu, N. Hao, Y. Y. Wang, C. Dou, F. Lin, R. Shen, R. Bura, D. B. Hodge, B. E. Dale, A. J. Ragauskas, B. Yang and J. S. Yuan, *Nat. Commun.*, 2021, **12**, 3912.
10 C. Yan, X. Jiang, J. Yu, Z. Ding, L. Ma, T. Su, Y. Wang, C. Wang, G. Huang and S. Xu, *Green Chem.*, 2023, **25**, 3816–3846.
11 S. C. Lee, S. H. Lee and K. Won, *Biotechnol. Bioprocess Eng.*, 2019, **24**, 258–263.
12 J. Kim, T. V. T. Nguyen, Y. H. Kim, F. Hollmann and C. B. Park, *Nat. Synth.*, 2022, **1**, 217–226.
13 K. O. Olatunji, N. A. Ahmed and O. Ogunkunle, *Biotechnol. Biofuels*, 2021, **14**, 159.
14 Q. Liu, T. Kawai, Y. Inukai, D. Aoki, Z. Feng, Y. Xiao, K. Fukushima, X. Lin, W. Shi, W. Busch, Y. Matsushita and B. Li, *Nat. Commun.*, 2023, **14**, 4866.
15 S. J. Freakley, S. Kochius, J. van Marwijk, C. Fenner, R. J. Lewis, K. Baldenius, S. S. Marais, D. J. Opperman, S. T. L. Harrison, M. Alcalde, M. S. Smit and G. J. Hutchings, *Nat. Commun.*, 2019, **10**, 4178.
16 E. Romero, M. J. Johansson, J. Cartwright, G. Grogan and M. A. Hayes, *Angew. Chem., Int. Ed.*, 2022, **61**, e202207831.
17 L. Rotilio, A. Swoboda, K. Ebner, C. Rinnofner, A. Glieder, W. Kroutil and A. Mattevi, *ACS Catal.*, 2021, **11**, 11511–11525.
18 S. Fang, X. Lyu, T. Tong, A. I. Lim, T. Li, J. Bao and Y. H. Hu, *Nat. Commun.*, 2023, **14**, 1203.
19 H. Kawana, T. Miwa, Y. Honda and T. Furuya, *ACS Omega*, 2022, **7**, 20259–20266.
20 M. M. C. H. van Schie, W. Zhang, F. Tieves, D. S. Choi, C. B. Park, B. O. Burek, J. Z. Bloh, I. W. C. E. Arends, C. E. Paul, M. Alcalde and F. Hollmann, *ACS Catal.*, 2019, **9**, 7409–7417.
21 F. Tonin, F. Tieves, S. Willot, A. van Troost, R. van Oosten, S. Breestraat, S. van Pelt, M. Alcalde and F. Hollmann, *Org. Process Res. Dev.*, 2021, **25**, 1414–1418.
22 A. Sluiter, B. Hames, R. Ruiz, C. Scarlata, J. Sluiter, D. Templeton and D. Crocker, Determination of structural carbohydrates and lignin in biomass, NREL/TP-510-42619, US National Renewable Energy Laboratory, Golden, Colorado, 2008, vol. 1617, pp. 1–16.

23 M. Toda, T. Akiyama, T. Yokoyama and Y. Matsumoto, *BioResources*, 2015, **10**, 2328–2337.
24 T. Chhabra, P. Dwivedi and V. Krishnan, *Green Chem.*, 2022, **24**, 898–910.
25 N. Kumari, T. Chhabra, S. Kumar and V. Krishnan, *Catal. Commun.*, 2022, **168**, 106467.
26 T. He, H. Tang, J. Wu, J. Wang, M. Zhang, C. Lu, H. Huang, J. Zhong, T. Cheng, Y. Liu and Z. Kang, *Nat. Commun.*, 2024, **15**, 7833.
27 N. Bryant, N. Engle, T. Tschaplinski, Y. Pu and A. J. Ragauskas, *RSC Adv.*, 2023, **13**, 20187–20197.
28 M. Toda, T. Akiyama, T. Yokoyama and Y. Matsumoto, *BioResources*, 2015, **10**, 2328–2337.
29 B. Jiang, T. Cao, F. Gu, W. Wu and Y. Jin, *ACS Sustainable Chem. Eng.*, 2016, **5**, 342–349.
30 A. Sluiter, B. Hames, R. Ruiz, C. Scarlata, J. Sluiter, D. Templeton and D. L. A. P. Crocker, *Lab. Anal. Proced.*, 2008, **1617**, 1–16.
31 Y. Wang, X. Liang, Y. Dai, L. Zou, D. Sun and F. Li, *RSC Adv.*, 2023, **13**, 25978–25988.
32 H. Zhou, H. Wang, C. Yue, L. He, H. Li, H. Zhang, S. Yang and T. Ma, *Appl. Catal., B*, 2024, (344), 123605.
33 C. Sandford, M. A. Edwards, K. J. Klunder, D. P. Hickey, M. Li, K. Barman, M. S. Sigman, H. S. White and S. D. Minteer, *Chem. Sci.*, 2019, **10**, 6404–6422.
34 P. Reddy, *S. Afr. J. Sci.*, 2015, **111**, 1–9.
35 M. Dash and K. Mohanty, *Biomass Bioenergy*, 2019, **124**, 33–42.
36 N. Corbin, J. Zeng, K. Williams and K. Manthiram, *Nano Res.*, 2019, **12**, 2093–2125.
37 S. Ren, E. W. Lees, C. Hunt, A. Jewlal, Y. Kim, Z. Zhang, B. A. W. Mowbray, A. G. Fink, L. Melo, E. R. Grant and C. P. Berlinguette, *J. Am. Chem. Soc.*, 2023, **145**, 4414–4420.
38 J. Jang, W. Aurangzeb Khan, F. Hollmann, K. Won and C. B. Park, *ACS Sustainable Chem. Eng.*, 2024, **12**, 8950–8957.
39 Z. Bao, J. Zhao, S. Zhang, L. Ding, X. Peng, G. Wang, Z. Zhao, X. Zhong, Z. Yao and J. Wang, *J. Mater. Chem. A*, 2022, **10**, 4749–4757.
40 Q. Zhang, L. Zheng, F. Gu, J. Wu, J. Gao, Y.-C. Zhang and X.-D. Zhu, *Nano Energy*, 2023, **116**, 108798.
41 C. H. Lee, J. Kim and C. B. Park, *ACS Energy Lett.*, 2023, **8**, 2513–2521.
42 T. Freese, J. T. Meijer, B. L. Feringa and S. B. Beil, *Nat. Catal.*, 2023, **6**, 553–558.
43 J. Marangon, H. D. Correia, C. D. Brondino, J. J. Moura, M. J. Romao, P. J. Gonzalez and T. Santos-Silva, *PLoS One*, 2013, **8**, e83234.
44 Y. Liu, X. Zhang and H. Liu, *RSC Adv.*, 2023, **13**, 34335–34347.
45 M. Hayyan, M. A. Hashim and I. M. AlNashef, *Chem. Rev.*, 2016, **116**, 3029–3085.
46 J.-C. Dong, X.-G. Zhang, V. Briega-Martos, X. Jin, J. Yang, S. Chen, Z.-L. Yang, D.-Y. Wu, J. M. Feliu, C. T. Williams, Z.-Q. Tian and J.-F. Li, *Nat. Energy*, 2018, **4**, 60–67.
47 D. S. Choi, H. Lee, F. Tieves, Y. W. Lee, E. J. Son, W. Zhang, B. Shin, F. Hollmann and C. B. Park, *ACS Catal.*, 2019, **9**, 10562–10566.
48 D. M. Schultz and T. P. Yoon, *Science*, 2014, **343**, 1239176.
49 E. G. Kommedal, C. F. Angeltveit, L. J. Klau, I. Ayuso-Fernandez, B. Arstad, S. G. Antonsen, Y. Stenstrom, D. Ekeberg, F. Girio, F. Carvalheiro, S. J. Horn, F. L. Aachmann and V. G. H. Eijsink, *Nat. Commun.*, 2023, **14**, 1063.
50 H. Guo, X. Luo, L. Wang, C. Yang, S. Li, S. Liu, J. Li and Z. Chen, *ChemSusChem*, 2025, **18**, e202402117.
51 C. M. Heckmann, M. Burgler and C. E. Paul, *ACS Catal.*, 2024, **14**, 2985–2991.
52 D. H. Knack, J. L. Marshall, G. P. Harlow, A. Dudzik, M. Szaleniec, S. Y. Liu and J. Heider, *Angew. Chem., Int. Ed.*, 2013, **52**, 2599–2601.
53 A. Rudzka, N. Antos, T. Reiter, W. Kroutil and P. Borowiecki, *ACS Catal.*, 2024, **14**, 1808–1823.

